NASA Technical Memorandum 105283

Unsteady-Flow-Field Predicitons for Oscillating Cascades

Dennis L. Huff
Lewis Research Center
Cleveland, Ohio

NASA

UNSTEADY FLOW-FIELD PREDICTIONS FOR OSCILLATING CASCADES

Dennis L. Huff
National Aeronautics and Space Administration
Lewis Research Center
Cleveland, Ohio 44135

SUMMARY

The unsteady flow field around an oscillating cascade of flat plates with zero stagger was investigated by using a time-marching Euler code. This case had an exact solution based on linear theory and served as a model problem for studying pressure wave propagation in the numerical solution. The importance of using proper unsteady boundary conditions, grid resolution, and time step size was demonstrated for a moderate reduced frequency. Results show that an approximate nonreflecting boundary condition based on linear theory does a good job of minimizing reflections from the inflow and outflow boundaries and allows the placement of the boundaries to be closer to the airfoils than when reflective boundary conditions are used. Stretching the boundary to dampen the unsteady waves is another way to minimize reflections. Grid clustering near the plates captures the unsteady flow field better than when uniform grids are used as long as the Courant-Friedrichs-Levy (CFL) number is less than 1 for a sufficient portion of the grid. Finally, a solution based on an optimization of grid, CFL number, and boundary conditions shows good agreement with linear theory.

INTRODUCTION

The accurate prediction of the unsteady flow field in turbomachinery remains a critical challenge in predicting noise and aeroelastic response. Advanced designs of ducted propellers for large commercial aircraft have relatively large shroud diameters and swept composite blades. The blades are expected to be more flexible than the blades used in current turbofans. Blade-row interaction effects will be important for both aeroelasticity and aeroacoustics. Analytical and experimental predictions of the unsteady aerodynamics associated with these designs are needed to ensure safe operation and lower noise.

Although three-dimensional methods are needed for a complete simulation of the unsteady flows associated with swept blades, two-dimensional analyses of linear cascades are used in practice. Aeroelastic and aeroacoustic analyses commonly model a single blade row responding to a gust or to blade vibration. A number of numerical and analytical methods are available for addressing the two-dimensional, oscillating cascade problem. Time-linearized analysis has been used the most because it performs reasonably well near design conditions and is inexpensive to compute. Also, exact specification of the inflow and outflow boundary conditions is possible. An assumption made with all of these methods is that the unsteady flow field is a small perturbation of the mean flow. Work in this category includes Smith (ref. 1), Whitehead (ref. 2), Verdon (ref. 3), Hall and Crawley (ref. 4), and Fang and Atassi (ref. 5). Time-marching, nonlinear schemes are also available that solve the full-potential (ref. 6), Euler (refs. 7 to 12), and Navier-Stokes (refs. 8 and 11) equations. These methods are needed for flows where small-perturbation approaches are no longer valid. However, they require larger amounts of computer time than linearized methods. In addition, proper treatment of the inflow and outflow boundary conditions, which is essential for accuracy, is difficult.

This study fundamentally investigated the unsteady flow field around an oscillating cascade by using a time-marching Euler code. The code solves the nonlinear Euler equations by using a high-resolution, wave-split scheme. Only linear solutions are sought for a simple cascade of flat plates. Although using an Euler code is overkill for this problem, an exact solution that is known from linear theory can be used as a baseline for code validation. Furthermore, fundamental studies of pressure wave propagation using a time-marching computational fluid dynamics (CFD) code are needed to better understand the limitations of numerical solutions. Choosing the proper grid resolution, time step size, and boundary conditions is important for resolving the unsteady flow field. Modeling the linear flow for oscillating flat plates is a first step toward validating a numerical solution to be used for aeroelasticity and aeroacoustics and must be done correctly before solutions for more complex flow fields can be considered accurate. This is particularly true for moderate blade passing frequencies associated with forced-response problems in aeroelasticity and with blade row interaction problems in aeroacoustics.

In the present work the numerical predictions of the unsteady aerodynamics of an unstaggered, oscillating cascade of flat plates were studied in detail. An unstaggered cascade was used so that the computational grid was perfectly orthogonal. An oscillation frequency was chosen that simulated a representative blade passing frequency in an advanced ducted propeller design. The importance of using the proper inflow and outflow boundary conditions was demonstrated. The effects of the boundary distance from the cascade, grid clustering, and time step size on the solution were investigated.

NOMENCLATURE

$\bar{A}$	Roe matrix
c	chord length, speed of sound, or unsteady characteristic variable
ΔCP	pressure difference coefficient, $(p_- - p_+)/(\rho_1 V_1^2 |h_1| k)$
e	energy
F,G	flux vectors
h_1	amplitude of oscillation for plunging motions based on chord length
$\mathcal{Im}\{\ \}$	imaginary part of $\{\ \}$
k	semichord reduced frequency, $\omega c/(2V_1^2)$
M	Mach number
p	static pressure
Q	dependent variable vector
$\mathcal{Re}\{\ \}$	real part of $\{\ \}$
t,τ	time
u,v	velocities in x,y directions, respectively
V	total velocity
x,y	spatial coordinates
ξ,η	curvilinear coordinate directions
ρ	fluid density

2

σ interblade phase angle

ω oscillation frequency

Subscripts:

1,2   conditions at inlet or exit

+,−   upper or lower surfaces on plate

L,R left or right of an interface

GOVERNING EQUATIONS AND NUMERICAL ALGORITHM

The unsteady, two-dimensional Euler equations written in conservative differential form are used and are transformed from a Cartesian to a time-dependent curvilinear reference frame. This transformation process and complete details of the numerical algorithm are presented in references 13 to 17. A brief overview is given here.

The transformed equations can be written in vector form as

$$\frac{\partial Q}{\partial \tau} + \frac{\partial F}{\partial \xi} + \frac{\partial G}{\partial \eta} = 0 \qquad (1)$$

where

$$Q = Jq \qquad (2a)$$

$$F = J(\xi_t q + \xi_x f + \xi_y g) \qquad (2b)$$

$$G = J(\eta_t q + \eta_x f + \eta_y g) \qquad (2c)$$

and

$$q = [\rho,\ \rho u,\ \rho v,\ e]^T \qquad (3a)$$

$$f = \left[\rho u,\ \rho u^2 + p,\ \rho u v,\ u(e + p)\right]^T \qquad (3b)$$

$$g = \left[\rho v,\ \rho u v,\ \rho v^2 + p,\ v(e + p)\right]^T \qquad (3c)$$

and

$\xi_t,\ \xi_x,\ \xi_y,\ \eta_t,\ \eta_x,$ and η_y are the metrics and J is the Jacobian of transformation.

These equations are discretized and solved by using a finite volume method, where cell centers are denoted as i and j:

$$\frac{\partial Q}{\partial \tau} + \frac{\delta_i F}{\Delta \xi} + \frac{\delta_j G}{\Delta \eta} = 0 \tag{4}$$

With $\Delta \xi = \Delta \eta = 1$ (by definition), this becomes

$$\frac{\partial Q}{\partial \tau} = -\left(\delta_i F + \delta_j G\right) \tag{5}$$

where

$$\delta_*(.) = (.)_{*+1/2} - (.)_{*-1/2} \tag{6}$$

The components of the dependent vector Q represent average values over a particular cell. However, a method is needed to allow these fluxes to be accurately represented at cell faces. As discussed in reference 13, the method used in the present effort is based on the one-dimensional approximate Riemann solver of Roe (ref. 18) at cell interfaces for each coordinate direction. The method uses an approximate equation to represent a quasilinear form of a locally one-dimensional conservation law:

$$\frac{\partial q}{\partial t} + \bar{A}(q_L, q_R)\frac{\partial q}{\partial x} = 0 \tag{7}$$

where $\bar{A}(q_L, q_R)$ is a constant matrix that is representative of local cell interface conditions and is constructed by using so-called "Roe averaged" variables. Determining the eigensystem of $\bar{A}$ and knowing that the change in dependent variables across an interface is proportional to the right eigenvectors allow first-order flux formulas to be constructed. This approach of extracting flow field information from characteristically dictated directions is commonly called flux difference splitting (FDS) and is applicable to multidimensional space, provided the assumption is made that all wave propagation occurs normal to a particular cell interface. In order to provide higher order spatial accuracy, a corrective flux is appended to this first-order flux. In addition, in order to control dispersive errors commonly encountered with higher order schemes, so-called limiters are used to limit components of the interface flux that result in total-variation-diminishing (TVD) schemes. All solutions presented herein were obtained by using the basic algorithm developed in reference 13, which is third-order accurate in space and second-order accurate in time.

GRID

For the simple flat-plate cascades considered in this study the flow equations were solved on Cartesian H-grids. Uniformly spaced grids were generated algebraically. Grids with cells clustered near the plates or grids coarsened near the inflow and outflow boundaries were

generated by using a two-dimensional version of the IGB code developed by Beach (ref. 19) for turbomachinery. This grid generator uses a hyperbolic tangent function to determine the spacing upstream and downstream of the cascade and ensures smooth variation in grid spacing. Once a grid is generated for a single passage, it is stacked to form a cascade with multiple passages.

All applications are for plunging motions of plates with an interblade phase angle σ of 90°. When the direct-store method presented in reference 12 is used, this requires four blade passages. The Euler code is blocked so that the passage-centered H-grids and the corresponding dependent variables are stored on a solid-state storage device (SSD) on the Cray computer; the computer retrieves the information as needed. Within one block the lower computational boundary contains the upper surface of one blade in the cascade, and the upper computational boundary contains the lower surface corresponding to the adjacent blade. The grid from each passage is deformed so that it follows the plunging motion near the plates and remains fixed near the center of the passage. This is done by using weighting functions and is described in more detail in reference 12. The code time-marches the grid and the flow solution for harmonic oscillations of the plates.

BOUNDARY CONDITIONS

Solid-Surface and Periodic Boundary Conditions

The solid-surface boundary conditions used in the present study were zero-pressure-gradient conditions. Janus (ref. 20) and others at Mississippi State University have found that zero-pressure-gradient boundary conditions are sufficient if the grid near the surface is adequately resolved. The boundaries that extend upstream and downstream of the plates are called periodic boundaries for plates with harmonic motion and a specified interblade phase angle. The Euler code stores phantom cells on either side of these boundaries and uses injection of the dependent variables to specify the boundary conditions for a given passage.

Steady Inflow and Outflow Boundary Conditions

The far-field, steady boundary conditions are based on characteristic variables and assume a locally one-dimensional flow at the boundary. A summary of their derivation that is based on reference 20 is given here.

For the sake of deriving the boundary conditions the Euler equations are written in their nonconservative form:

$$\frac{\partial q}{\partial \tau} + a \frac{\partial q}{\partial \xi} + b \frac{\partial q}{\partial \eta} = 0 \tag{8}$$

The matrices a and b are determined through an eigenvalue analysis. Multiplying by P_ξ^{-1} and neglecting the derivatives in the η direction gives

5

$$P_\xi^{-1} \frac{\partial q}{\partial \tau} + P_\xi^{-1} P_\xi \Lambda_\xi P_\xi^{-1} \frac{\partial q}{\partial \xi} = 0 \qquad (9)$$

where Λ_ξ is a diagonal matrix containing the eigenvalues λ_ξ; and P_ξ and P_ξ^{-1} are the left and right eigenvectors, respectively. The characteristic vector is defined as

$$W_\xi = P_\xi^{-1} q \qquad (10)$$

where P_ξ is derived in reference 20 so that the elements of the characteristic vector become

$$w_\xi^1 = \frac{J}{|\nabla \xi|}\left[\xi_x\left(\rho - \frac{p}{c_1^2}\right)\right] \qquad (11a)$$

$$w_\xi^2 = \frac{J}{|\nabla \xi|}\left[\xi_y\left(\rho - \frac{p}{c_1^2}\right)\right] \qquad (11b)$$

$$w_\xi^3 = \frac{J}{\sqrt{2}|\nabla \xi|}\left[\frac{p|\nabla \xi|}{\rho_1 c_1} + (\xi_x u + \xi_y v)\right] \qquad (11c)$$

$$w_\xi^4 = \frac{J}{\sqrt{2}|\nabla \xi|}\left[\frac{p|\nabla \xi|}{\rho_1 c_1} - (\xi_x u + \xi_y v)\right] \qquad (11d)$$

The corresponding eigenvalues are

$$\lambda_\xi^1, \lambda_\xi^2 = \xi_t + \xi_x u + \xi_y v \qquad (12a,b)$$

$$\lambda_\xi^3 = (\xi_x u + \xi_y v) + c|\nabla \xi| \qquad (12c)$$

$$\lambda_\xi^4 = (\xi_x u + \xi_y v) - c|\nabla \xi| \qquad (12d)$$

The implementation of the characteristic variable boundary conditions requires knowing if the boundary is an inflow or an outflow. Generally, this is found by computing the sign of λ to determine the directions of the characteristics. However, for cascades the direction of the flow and the characteristics at the boundaries are known. Let the subscript a denote approaching a boundary, b denote being on the boundary, and l denote leaving the boundary. For a subsonic inflow the characteristics approaching the boundary are set equal to the characteristics on the boundary by using equation (11).

$$\left[\xi_x\left(\rho - \frac{p}{c_1^2}\right)\right]_a = \left[\xi_x\left(\rho - \frac{p}{c_1^2}\right)\right]_b \tag{13a}$$

$$\left[\xi_y\left(\rho - \frac{p}{c_1^2}\right)\right]_a = \left[\xi_y\left(\rho - \frac{p}{c_1^2}\right)\right]_b \tag{13b}$$

$$\left[\frac{p|\nabla\xi|}{\rho_1 c_1} + (\xi_x u + \xi_y v)\right]_a = \left[\frac{p|\nabla\xi|}{\rho_1 c_1} + (\xi_x u + \xi_y v)\right]_b \tag{13c}$$

$$\left[\frac{p|\nabla\xi|}{\rho_1 c_1} - (\xi_x u + \xi_y v)\right]_l = \left[\frac{p|\nabla\xi|}{\rho_1 c_1} - (\xi_x u + \xi_y v)\right]_b \tag{13d}$$

Solving equations (13a) to (13d) while assuming that the metrics at the boundary are equal to the metrics at a and l, gives the following information for the flow variables at the inflow boundary:

$$p_b = \frac{1}{2}\{p_a + p_l + \rho_1 c_1[\xi_x(u_a - u_l) + \xi_y(v_a - v_l)]\} \tag{14a}$$

$$\rho_b = \rho_a + \frac{p_b - p_a}{c_1^2} \tag{14b}$$

$$u_b = u_a + \xi_x \frac{p_a - p_b}{\rho_1 c_1} \tag{14c}$$

$$v_b = v_a + \xi_y \frac{p_a - p_b}{\rho_1 c_1} \tag{14d}$$

With the nonconservative flow variables known, the conservative dependent variables (eq. (3a)) can be easily computed at the boundary.

The flow variables at the outflow boundary are found in a similar manner. The characteristics on the boundary are set equal to the characteristics leaving the boundary. In this case the incoming characteristic is the upstream-running pressure wave, and therefore the pressure is set equal to the pressure at l. For internal steady flows the pressure is usually specified by the user. The nonconservative flow variables become

$$p_b = p_l \tag{15a}$$

7

$$\rho_b = \rho_a + \frac{p_b - p_a}{c_2^2} \qquad (15b)$$

$$u_b = u_a + \xi_x \frac{p_a - p_b}{\rho_2 c_2} \qquad (15c)$$

$$v_b = v_a + \xi_y \frac{p_a - p_b}{\rho_2 c_2} \qquad (15d)$$

These characteristic variable boundary conditions are valid only for steady flows when applied to cascades because the outflow is assumed to have uniform static pressure. A number of flow solvers today mistakenly use similar boundary conditions for unsteady flows. For comparison purposes these boundary conditions will be called reflective boundary conditions when they are used later for unsteady flows. A better approximation for the correct unsteady boundary conditions is examined next.

Unsteady Inflow and Outflow Boundary Conditions

For unsteady flows in turbomachinery the exact specification of the unsteady boundary conditions for nonlinear problems is not feasible. Approximate "nonreflecting" boundary conditions are developed by assuming that linear theory can be applied. A very useful publication by Giles (ref. 21) presents the formulation of boundary conditions for internal flows. Much of the original theoretical work on this topic was done by Kreiss (ref. 22). Giles has transformed the theory into a form that can be easily implemented in general Euler solvers for turbomachinery. The basic implementation of this formulation determines the steady flow by using the boundary conditions derived herein and then solves the time-linearized form of the Euler equations at the boundary to determine the perturbation flow variables in terms of the characteristic variables. This implementation allows time variations of static pressure at the outflow and reduces reflections from the boundaries. A brief summary that is based on reference 21 is given next.

For the cases considered in this paper, $x = \xi$, $y = \eta$, and $t = \tau$, so that the primitive form of the Euler equations can be written as

$$\frac{\partial U}{\partial t} + A \frac{\partial U}{\partial x} + B \frac{\partial U}{\partial y} = 0 \qquad (16)$$

where

$$U = (\rho, u, v, p)^T \qquad (17a)$$

8

$$A = \begin{pmatrix} u & \rho & 0 & 0 \\ 0 & u & 0 & \dfrac{1}{\rho} \\ 0 & 0 & u & 0 \\ 0 & \gamma p & 0 & u \end{pmatrix}$$

(17b)

$$B = \begin{pmatrix} v & 0 & \rho & 0 \\ 0 & v & 0 & 0 \\ 0 & 0 & v & \dfrac{1}{\rho} \\ 0 & 0 & \gamma p & v \end{pmatrix}$$

(17c)

For small perturbations from the steady flow and with higher order terms neglected, a linear form of the Euler equations can be written as

$$\frac{\partial U'}{\partial t} + A\frac{\partial U'}{\partial x} + B\frac{\partial U'}{\partial y} = 0$$

(18)

where U' are the perturbation variables given as

$$U' = (\tilde{\rho}, \tilde{u}, \tilde{v}, \tilde{p})^T$$

(17a)

and A,B are constant coefficient matrices based on the steady flow variables. The nondimensional form of these matrices is

$$A = \begin{pmatrix} u & 1 & 0 & 0 \\ 0 & u & 0 & 1 \\ 0 & 0 & u & 0 \\ 0 & 1 & 0 & u \end{pmatrix}$$

(18a)

$$B = \begin{pmatrix} v & 0 & 1 & 0 \\ 0 & v & 0 & 0 \\ 0 & 0 & v & 1 \\ 0 & 0 & 1 & v \end{pmatrix}$$

(18b)

Following a Fourier analysis of these equations, a set of eigenvectors representing an entropy wave, a vorticity wave, and upstream- or downstream-running pressure waves can be determined. The details of this procedure are given in reference 21. By using these eigenvectors and assuming locally one-dimensional flow at the boundary, the characteristic variables for unsteady flows are written in terms of the perturbation variables as

9

$$\begin{pmatrix} c_1 \\ c_2 \\ c_3 \\ c_4 \end{pmatrix} = \begin{pmatrix} -1 & 0 & 0 & 1 \\ 0 & 0 & 1 & 0 \\ 0 & 1 & 0 & 1 \\ 0 & -1 & 0 & 1 \end{pmatrix} \begin{pmatrix} \delta\rho \\ \delta u \\ \delta v \\ \delta p \end{pmatrix} \qquad (19)$$

where $\delta\rho$, δu, δv, and δp are the perturbations from the steady flow.

For a subsonic inflow the amplitudes of the incoming unsteady characteristics (c_1, c_2, c_3) are set to zero and the outgoing characteristic (c_4) is computed by using equation (19). For subsonic outflow $c_4 = 0$ and the remaining characteristics are computed. Once the characteristics are known, the perturbation variables are found by using an inverse transform:

$$\begin{pmatrix} \delta\rho \\ \delta u \\ \delta v \\ \delta p \end{pmatrix} = \begin{pmatrix} -1 & 0 & \dfrac{1}{2} & \dfrac{1}{2} \\ 0 & 0 & \dfrac{1}{2} & -\dfrac{1}{2} \\ 0 & 1 & 0 & 0 \\ 0 & 0 & \dfrac{1}{2} & \dfrac{1}{2} \end{pmatrix} \begin{pmatrix} c_1 \\ c_2 \\ c_3 \\ c_4 \end{pmatrix} \qquad (20)$$

The primitive flow variables can be found by using the following relationships:

$$\rho = \rho_0 + \delta\rho \qquad (21a)$$

$$u = u_0 + \delta u \qquad (21b)$$

$$v = v_0 + \delta v \qquad (21c)$$

$$p = p_0 + \delta p \qquad (21d)$$

where ρ_0, u_0, v_0, and p_0 are determined from the steady solution. Equation (3a) is then used to determine the conservative flow variables at the boundaries.

RESULTS AND DISCUSSION

A cascade of flat plates was used for studying the unsteady flow field caused by small-amplitude plunging motions. The purpose of the plunging motions is to propagate pressure waves upstream and downstream so that the accuracy of the CFD code in resolving the unsteady aerodynamics can be studied. Results are presented for one flow condition and various numerical conditions, such as inflow and outflow boundary conditions, grids, and time steps (CFL numbers). Although the blade vibration problem is usually associated with flutter analysis, the forcing frequencies considered were high enough to simulate forced-response problems. The small

disturbances introduced by the plate motion allow for comparisons with small-perturbation theory.

Model Problem

The flat-plate cascade geometry used in the present study is shown in figure 1(a). The stagger angle was 0° and the gap-to-chord ratio was 1. Uniform flow with M_1 = 0.50 was used for the steady flow. Small plunging oscillations with h_1 = 0.001 and σ = 90° were used for all of the cases presented. A semichord reduced frequency k of 4 was chosen to simulate a realistic rotor-stator frequency in advanced ducted propeller designs. According to linear theory this flow condition propagates single-mode pressure waves both upstream and downstream in a direction not aligned with the Cartesian grids. These conditions define a model problem with a known solution that can be used to study wave dynamics by using CFD.

The procedure used in the time-marching Euler code was to first determine a steady solution with no blade motion. For flat plates with zero incidence this solution reduced to uniform flow and could be specified analytically. The unsteady solutions were started with each plate moving according to the specified interblade phase angle. Unless specified otherwise, the maximum CFL number used in each of the following solutions was 1. The solution was run until the unsteady flow field reached periodicity. For the present study the unsteady pressures on the plate were Fourier transformed into their real and imaginary parts after each cycle of oscillation. The solution was stopped when the coefficients from the first harmonic did not vary significantly. This usually took 3 to 20 cycles of plate oscillation. The solutions presented herein were done on a CRAY YMP computer and took anywhere from 20 minutes to 5 hours of CPU time, depending on the grid and the time step.

Visualization of Effects of Boundary Conditions

A set of runs was done to visually demonstrate pressure wave propagation and the importance of using correct inflow and outflow unsteady boundary conditions. Consider a uniformly spaced grid (dx = dy = 0.05 chord length) with the inflow and outflow boundaries located six chord lengths away from the leading and trailing edges, respectively. The grid resolution is too coarse for accurate computation of surface pressures but should be sufficient for visual demonstration of pressure wave propagation to the far field. Figures 1(b) to (f) show "snapshots" of pressure contours just after the plates were impulsively moved from uniform flow. The amount of time between snapshots was approximately constant and is arbitrarily denoted by ΔT, which gives five instantaneous pressure plots over enough time for the downstream-running wave to reach the boundary. The left block used the "reflective" boundary conditions and the right block used the nonreflective boundary conditions. Because the reflective boundary conditions enforce constant static pressure at the outflow boundary, the downstream-running wave was reflected (figs. 1(e) and (f)). As the solution continued, the downstream domain was contaminated with an upstream-running wave that was nonphysical for the desired solution. With proper grid resolution this wave entered the cascade and affected the unsteady pressures on the plates.

Figure 2 shows the unsteady pressure distributions on the plate after the solution had run for 20 plate oscillation cycles. Four solutions are shown; two used the uniform grid with the reflective and nonreflective boundary conditions shown in figure 1 and the remaining two

solutions used the reflective boundary conditions on grids that coarsened as they extended to the inflow and outflow boundaries. Coarsening the grid introduced numerical dissipation into the solution that dampened the waves as they propagated. (This type of grid has been commonly used for isolated airfoil analysis.) The grid had been coarsened so that the resolution in the passage stayed the same ($dx = dy = 0.05$ chord length), but the aspect ratio of the cells gradually changed to 3:1 ($dx = 0.15$, $dy = 0.05$) at the inflow and outflow boundaries in one case and to 10:1 ($dx = 0.50$, $dy = 0.05$) in the other case. There was a significant difference between the reflective and nonreflective cases that used a uniform grid, as would be expected from the contour plots in figure 1. Also, the solutions that used the grid-coarsening technique and reflective boundary conditions tended toward those for the nonreflective boundary condition case that used a uniform grid. It is expected that grid coarsening will only work if the grid spacing variation is smooth because abrupt changes in the grid may cause internal reflections.

Effect of Boundary Distance From Cascade

The effect of inflow and outflow boundary distance from the cascade was investigated by using both the reflective and nonreflective boundary conditions. The upstream and downstream boundaries were placed 0.25, 0.5, 1.0, 1.5, and 2.0 chord lengths away from the leading and trailing edges of the plates, respectively. The grid density was refined to $dx = dy = 0.02$ chord length. Each case was run through 20 oscillation cycles to give the unsteady pressure predictions shown in figures 3 and 4. The results for the reflective boundary conditions (fig. 3) never reached a solution that was independent of the boundary distance. In contrast, the results for the nonreflective boundary conditions (fig. 4) were nearly identical when the boundaries were 1.5 and 2.0 chord lengths away from the cascade. Thus, using nonreflective boundary conditions can reduce the computational domain.

Results from linear theory (ref. 1) are also plotted in figures 3 and 4. The nonreflective boundary condition results that are independent of the boundary distance are in general but not exact agreement with the theory (short dashed lines in fig. 4). Because the theory is exact for flat plates, the differences between the solutions are due to numerical error. As demonstrated in the next section, the discrepancies are due to grid resolution. For now, the effects of boundary distance for different inflow and outflow boundary conditions determined in this study should still be valid.

Effect of Boundary Conditions With Grid Coarsening

The results shown in figure 2 have already demonstrated that the pressure waves by coarsening the grid should render a solution insensitive to either reflective or nonreflective boundary conditions. In order to verify this, another set of solutions was considered that used a finer grid near the plates which smoothly coarsened to the inflow and outflow boundaries. The same boundary distances of 6 chord lengths upstream and downstream were used. The grid density was $dx = dy = 0.02$ chord length in the passage and coarsened to $dx = 0.50$ and $dy = 0.02$ chord length at the inflow and outflow boundaries. The unsteady pressure distributions are plotted in figure 5 for solutions that used both the reflective and nonreflective boundary conditions, along with the exact solution from linear theory. The solutions were identical and differed from the theory by the same amount found in figure 4 for the nonreflective boundary conditions. Therefore, a solution has been found that is not influenced by reflections from the inflow and outflow boundaries.

Effect of Time Step (CFL Number)

All of the previous solutions were run with a maximum CFL number of 1. For cases with varying grid spacing this means that the smallest cell did not exceed a CFL number of 1 and the larger cells had a CFL number less than 1. Grids with uniform spacing had a CFL number of 1 for every cell. Specifying a maximum CFL number of 1 preserved, at least formally, the second-order temporal accuracy of the numerical solution. However, many unsteady solutions that use a time-marching code run higher CFL numbers to reduce the run times. When this is done, an assumption is made that the higher CFL numbers occur only at the smaller cells and do not significantly affect the global solution. The following solutions show how wrong this assumption can be if care is not taken to ensure that the CFL number is small enough to resolve the unsteady flow field.

The effects of CFL number were studied on two types of grid, including a uniformly spaced grid and a grid with points clustered near the plates. The nonreflecting boundary conditions were used in all of the remaining results. The uniformly spaced grid (dx = dy = 0.02 chord length) was identical to the one used in the study of boundary distance effects with the boundary located 0.5 chord length away from the cascade (figs. 3 and 4). Unsteady pressure predictions for three CFL numbers are shown in figure 6. The results for a CFL number of 1 are the same as those shown in figure 4. The good agreement with linear theory is fortuitous because the predictions for a boundary distance of 0.5 chord length were found to be insufficient. Increasing the CFL number to 2 and 3 introduced temporal error, as expected. Using a CFL number of 3 completely destroyed the character of the unsteady waveforms. For this case two solutions have been plotted after 20 and 40 cycles of plate oscillation to verify that the solution has reached periodicity.

A similar study is shown in figure 7 for a grid that was clustered in the y direction. The spacing near the plates was dx = 0.05, dy = 0.02 chord length and smoothly varied to a spacing of dx = dy = 0.05 chord length at the center of the passage. Hence, the maximum CFL number occurred near the plates. The boundary distance was 0.5 chord length upstream and downstream of the cascade. From the predictions shown in figure 7, clustering the grid near the surface helped preserve the character of the pressure waves but still quickly lost accuracy for maximum CFL numbers of 2 and 3. Note that for a maximum CFL number of 3, the minimum CFL number is 0.4 on this grid. This means that a portion of the grid should convect disturbances correctly near the center of the passage. However, in the region of the grid near the plates, which was where the unsteady disturbances were being generated, the correct magnitude and phase were not computed. This is the reason why, although the nature of the disturbance is captured with a clustered grid, the accuracy is poor for higher CFL numbers. As demonstrated in the next section, it is possible for highly clustered grids to do a reasonably good job of predicting the unsteady flow field provided that an adequate portion of the grid has a CFL number less than 1.

An Optimal Solution

Finally, using the studies presented herein, an optimal solution is presented in figure 8. A highly clustered grid near the leading and trailing edges (dx = 0.003, dy = 0.001 chord length) was used. The 121- by 41-grid (x by y) was stretched 6 chord lengths upstream and downstream of the cascade by using the grid-coarsening technique. The maximum CFL number was 10, which occurred near the leading and trailing edges of the plates. The CFL number quickly

13

diminished to less than 1 away from the plates, leaving a large percentage of the grid with an adequate time step to resolve the unsteady flow. Comparison of the unsteady pressure distributions with linear theory in figure 8 shows good agreement for most of the chord length.

CONCLUSIONS

A fundamental investigation of the unsteady flow field around an oscillating cascade of flat plates with zero stagger was done by using a time-marching Euler code. The study demonstrated the importance of using proper unsteady boundary conditions, grid resolution, and time step size to accurately model the unsteady flow field. Imposing constant static pressure across the outflow caused reflections from the downstream boundary and was shown by plotting pressure contours at various times. These reflections contaminated the unsteady pressure distributions on the plates. A study of the effect of boundary distance showed that the unsteady plate pressures never reached a solution that was independent of boundary distance. Using approximate nonreflecting boundary conditions based on linear theory improved the solutions and allowed the boundaries to be placed closer to the cascade (approximately 1.5 to 2 chord lengths away from the cascade). Coarsening the grid by stretching the boundaries away from the cascade introduced numerical damping to the solutions and was also an effective way to obtain correct unsteady surface pressures on the plates, although it was only valid for unsteady flows that are due to plate motion. These solutions were insensitive to reflecting or nonreflecting boundary conditions. Several solutions were presented that varied the time step size on both a clustered grid and a uniformly spaced grid. The results showed that the unsteady flow field became significantly inaccurate as the Courant-Friedrichs-Levy (CFL) number exceeded 1 on a uniformly spaced grid. The clustered grid results did a better job of capturing the flow but were still inaccurate because fewer grid cells had a CFL number less than 1. Good agreement with linear theory was found by using nonreflective boundary conditions on a highly clustered grid that stretched 6 chord lengths upstream and downstream from the cascade. For this case the maximum CFL number was 10 and quickly diminished to less than 1 away from the plates.

ACKNOWLEDGMENTS

REFERENCES

1. Smith, S.N.: Discrete Frequency Sound Generation in Axial Flow Turbomachines. ARC-R/M-3709, 1971. (Avail. NTIS, 73N22240.)

2. Whitehead, D.S.: Classical Two-Dimensional Methods. Aeroelasticity in Axial-Flow Turbomachines, Vol. 1, Unsteady Turbomachinery Aerodynamics, M.F. Platzer and F.O. Carta, eds. AGARDograph No. 298, 1987, pp. 3-1 to 3-30.

3. Verdon, J.M.; and Caspar, J.R.: A Linearized Unsteady Aerodynamic Analysis for Transonic Cascades. J. Fluid Mech., vol. 149, Dec. 1984, pp. 403-429.

4. Hall, K.C.; and Crawley, E.F.: Calculation of Unsteady Euler Flows in Turbomachinery Using the Linearized Euler Equations. Fourth Symposium on Unsteady Aerodynamics and Aeroelasticity of Turbomachines and Propellers, H.E. Gallus and S. Servaty, eds., Rheinisch-Westfaelische Technische Hochschule, Aachen, West Germany, 1987, pp. 15-38.

5. Fang, J.; and Atassi, H.M.: Compressible Flows With Vortical Disturbances Around a Cascade of Loaded Airfoils. Sixth Symposium on Unsteady Aerodynamics and Aeroelasticity of Turbomachines and Propellers, University of Notre Dame, Sept. 1991.

6. Kao, Y.F.: A Two-Dimensional Unsteady Analysis for Transonic and Supersonic Cascade Flows. Ph.D. Thesis, Purdue University, 1989.

7. Fransson, T.H.; and Pandolfi, M.: Numerical Investigation of Unsteady Subsonic Compressible Flows Through an Oscillating Cascade. ASME Paper 86-GT-304, June 1986.

8. Huff, D.L.: Numerical Analysis of Flow Through Oscillating Cascade Sections. AIAA Paper 89-0437, Jan. 1989. (Also, NASA TM-101417.)

9. He, L.: An Euler Solution for Unsteady Flows Around Oscillating Blades. J. Turbomachinery, vol. 112, no. 4, Oct. 1990, pp. 714-722.

10. Gerolymos, G.A.; Blin, E.; and Quiniou, H.: Comparison of Inviscid Computations With Theory and Experiment in Vibrating Transonic Compressor Cascades. ASME Paper 90-GT-373, June 1990.

11. Giles, M.; and Haimes, R.: Validation of a Numerical Method for Unsteady Flow Calculations. ASME Paper 91-GT-271, June 1991.

12. Huff, D.L.; Swafford, T.W.; and Reddy, T.S.R.: Euler Flow Predictions for an Oscillating Cascade Using a High Resolution Wave-Split Scheme. ASME Paper 91-GT-198, June 1991. (Also, NASA TM-104377.)

13. Whitfield, D.L.; Janus, J.M.; and Simpson, L.B.: Implicit Finite Volume High Resolution Wave-Split Scheme for Solving the Unsteady Three-Dimensional Euler and Navier-Stokes Equations on Stationary or Dynamic Grids. Mississippi State University, Engineering and Industrial Research Station, Report No. MSSU-EIRS-ASE-88-2, Feb. 1988.

14. Prewitt, N.C.: Two-Dimensional Euler Code for the Prediction of Pressure Distributions About an Airfoil. M.S. Thesis, Mississippi State University, 1988.

15. Janus, J.M.: Advanced 3-D CFD Algorithm for Turbomachinery. Ph.D. Dissertation, Mississippi State University, 1989.

16. Arabshahi, A.: A Dynamic Multiblock Approach to Solving the Unsteady Euler Equations About Complex Configurations. Ph.D. Dissertation, Mississippi State University, 1989.

17. Whitfield, D.L.; Janus, J.M.; and Arabshahi, A.: Unsteady Euler Solutions on Dynamic Blocked Grids for Complex Configurations. Applications of Mesh Generation to Complex 3-D Configurations, AGARD CP-464, 1990, pp. 7-1 to 7-13.

18. Roe, P.L.; Approximate Riemann Solvers, Parameter Vectors, and Difference Schemes. J. Comput. Phys., vol. 43, 1981, pp. 357-372.

19. Beach, T.A.: An Interactive Grid Generation Procedure for Axial and Radial Flow Turbomachinery. AIAA Paper 90-0344, Jan. 1990. (Also, NASA CR-185167.)

20. Janus, J.M.: The Development of a Three-Dimensional Split Flux Vector Solver With Dynamic Grid Applications. M.S. Thesis, Mississippi State University, 1984.

21. Giles, M.: Non-Reflecting Boundary Conditions for Euler Equation Calculations. 9th AIAA Computational Fluid Dynamics Conference, AIAA, 1989, pp. 143-153.

22. Kreiss, H.O.: Initial Boundary Value Problems for Hyperbolic Systems. Commun. Pure Appl. Math., vol. 23, 1970, pp. 277-298.
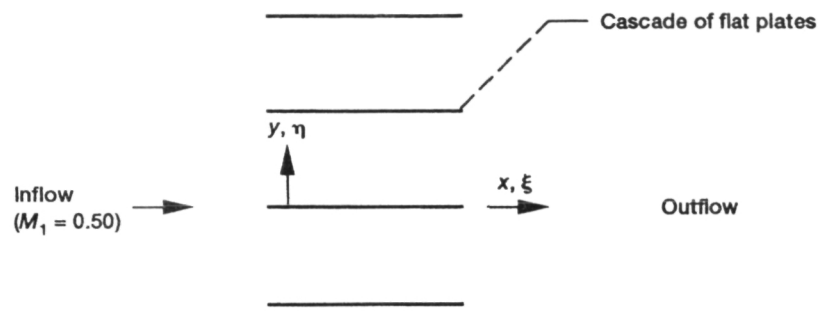
(a) Cascade geometry for model problem.

Reflective   Nonreflective
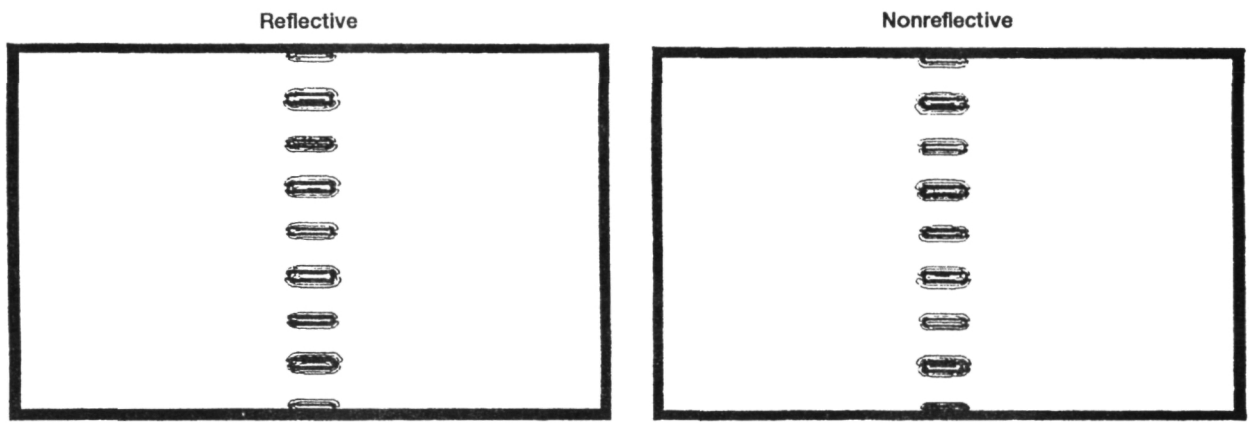
(b) $t > 0$.
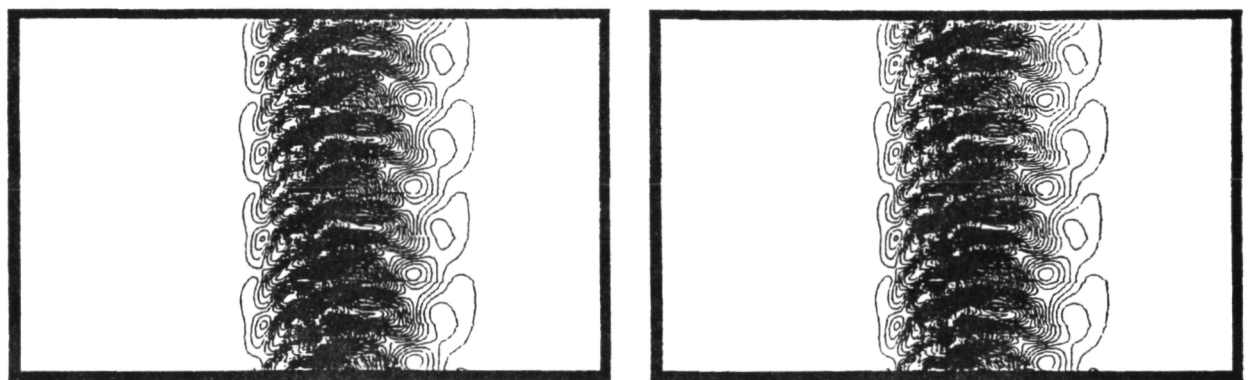
(c) $t = \Delta T$.

Figure 1.—Cascade geometry and instantaneous static pressures for model problem.

17

Reflective   Nonreflective
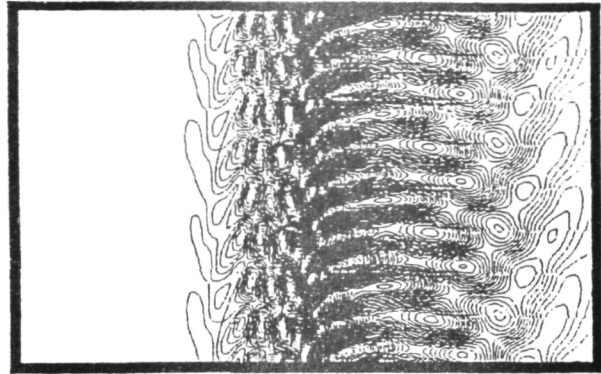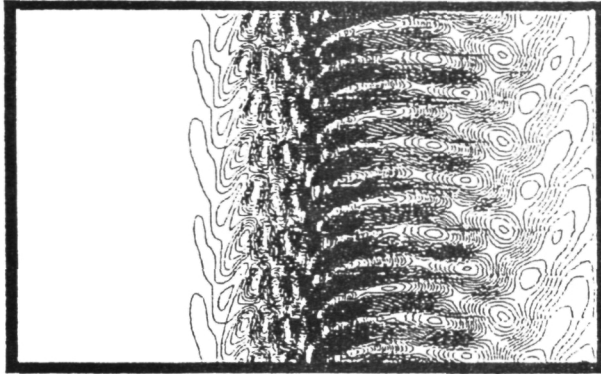
(d) $t = 2\Delta T$.
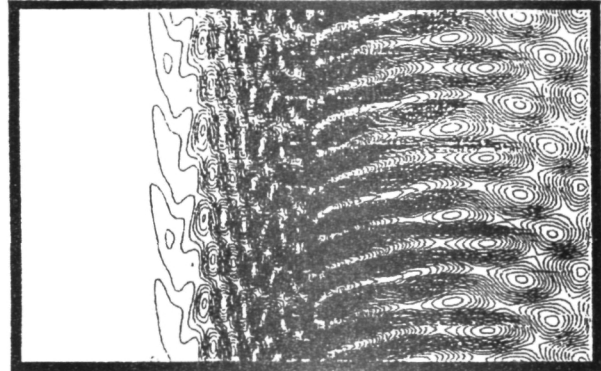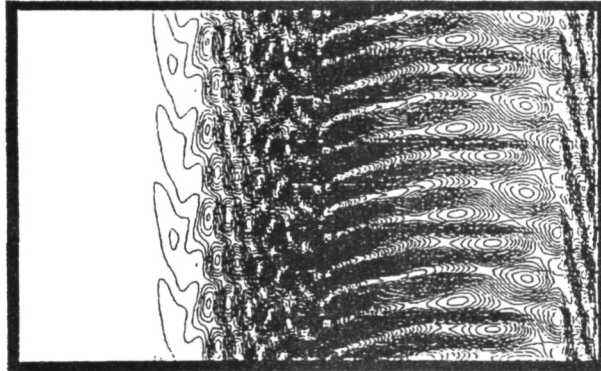
(e) $t = 3\Delta T$.
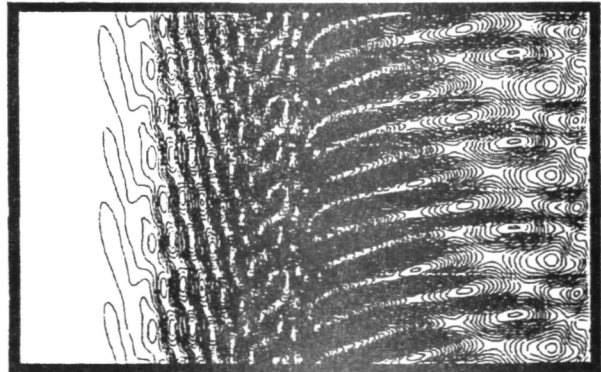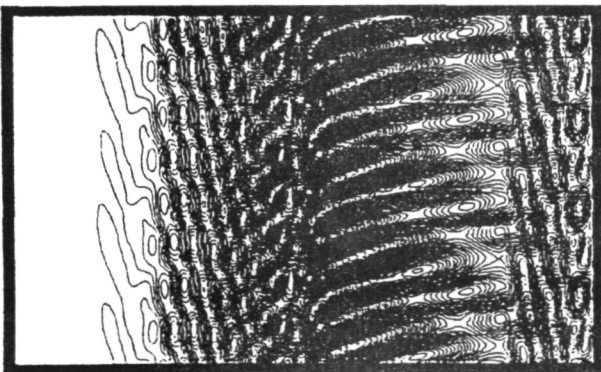
(f) $t = 4\Delta T$.

Figure 1.—Concluded.
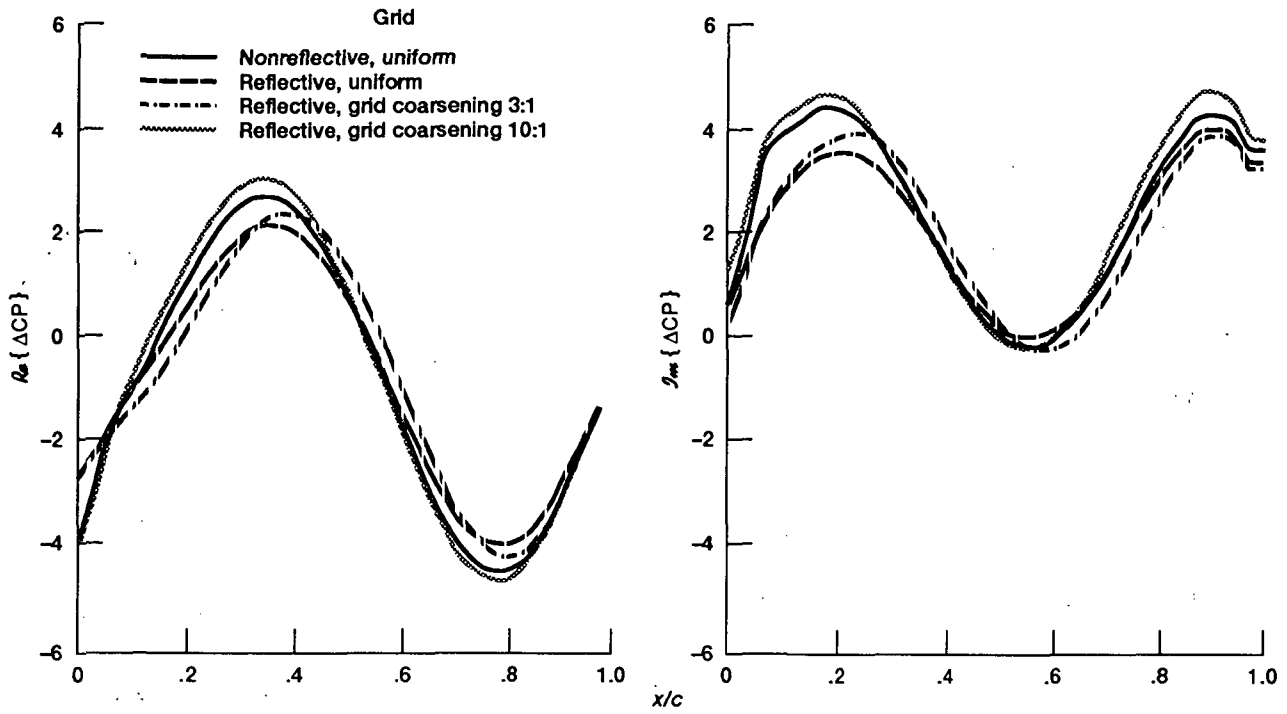
Figure 2.—Effects of boundary conditions and grid on unsteady pressure distributions.
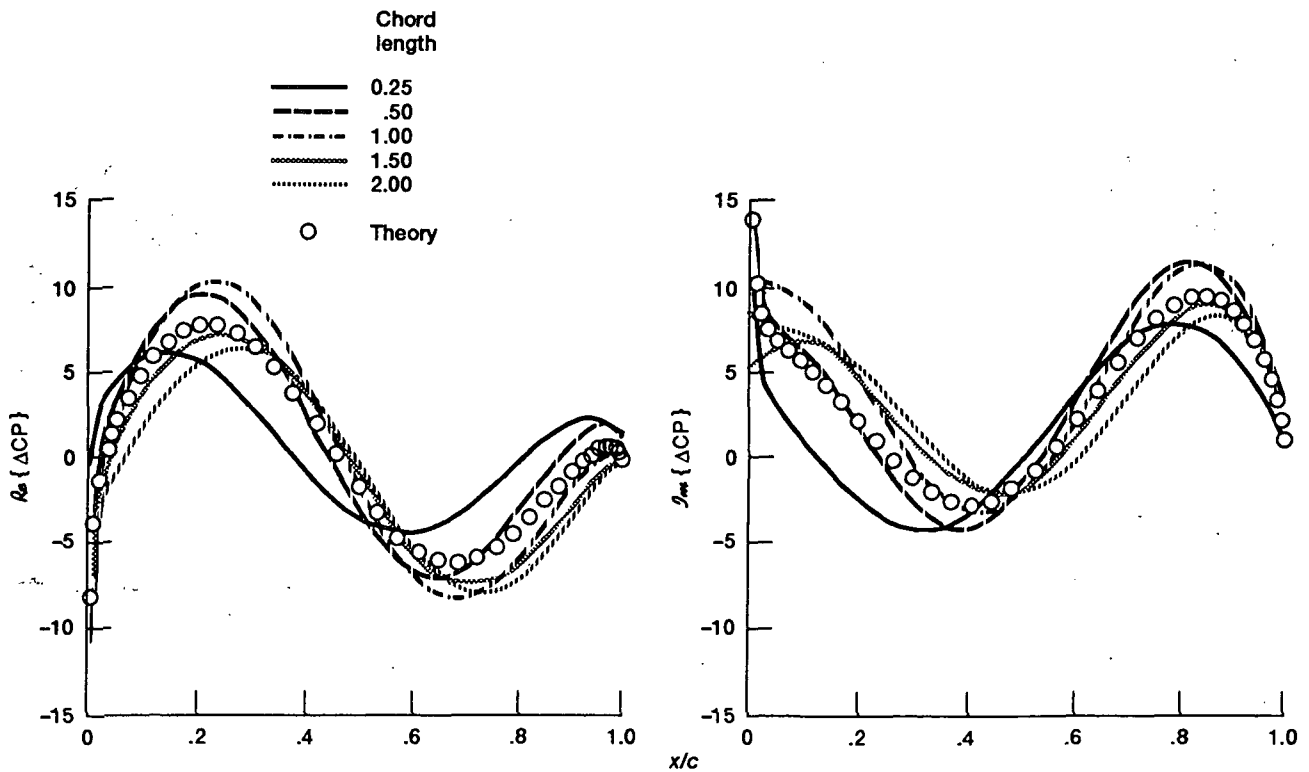
Figure 3.—Effects of boundary distance when reflective boundary conditions and Euler code are used.
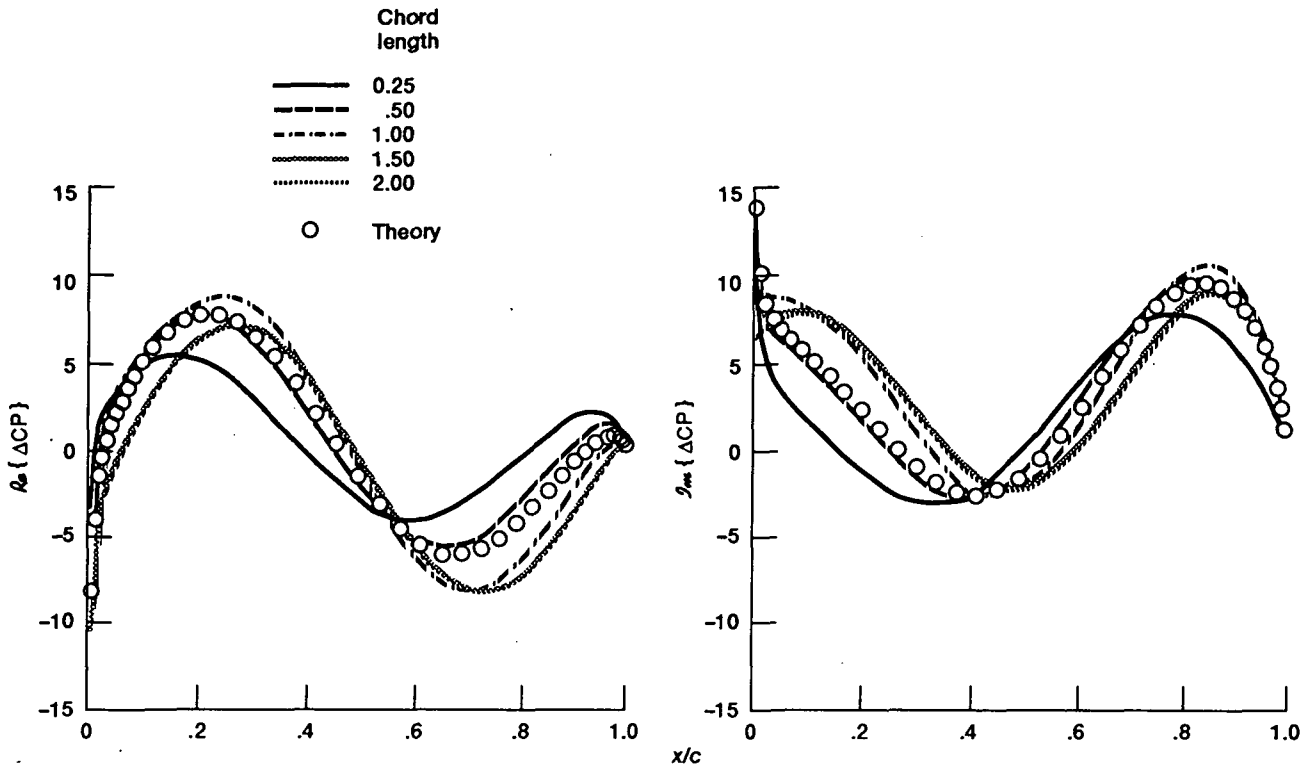
Figure 4.—Effects of boundary distance when nonreflective boundary conditions and Euler code are used.
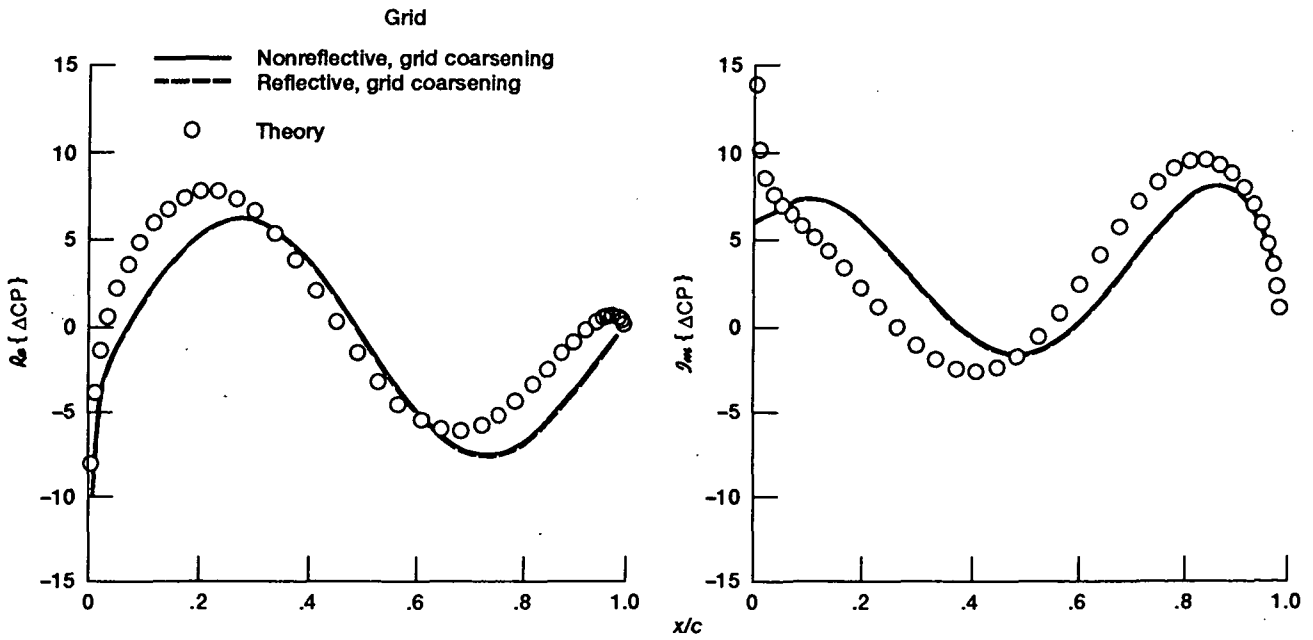
Figure 5.—Effects of boundary conditions on unsteady pressure distributions when grid coarsening is used.

20
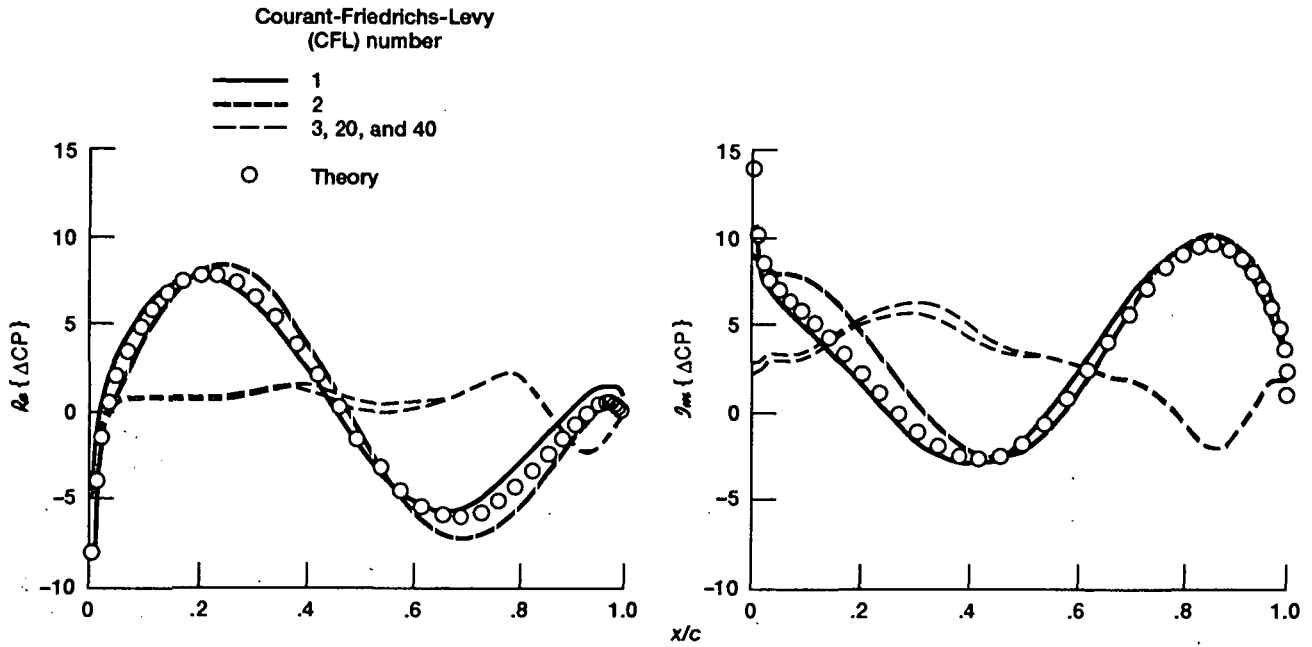
Figure 6.—Effects of time step on unsteady pressure distributions when a uniform grid is used.
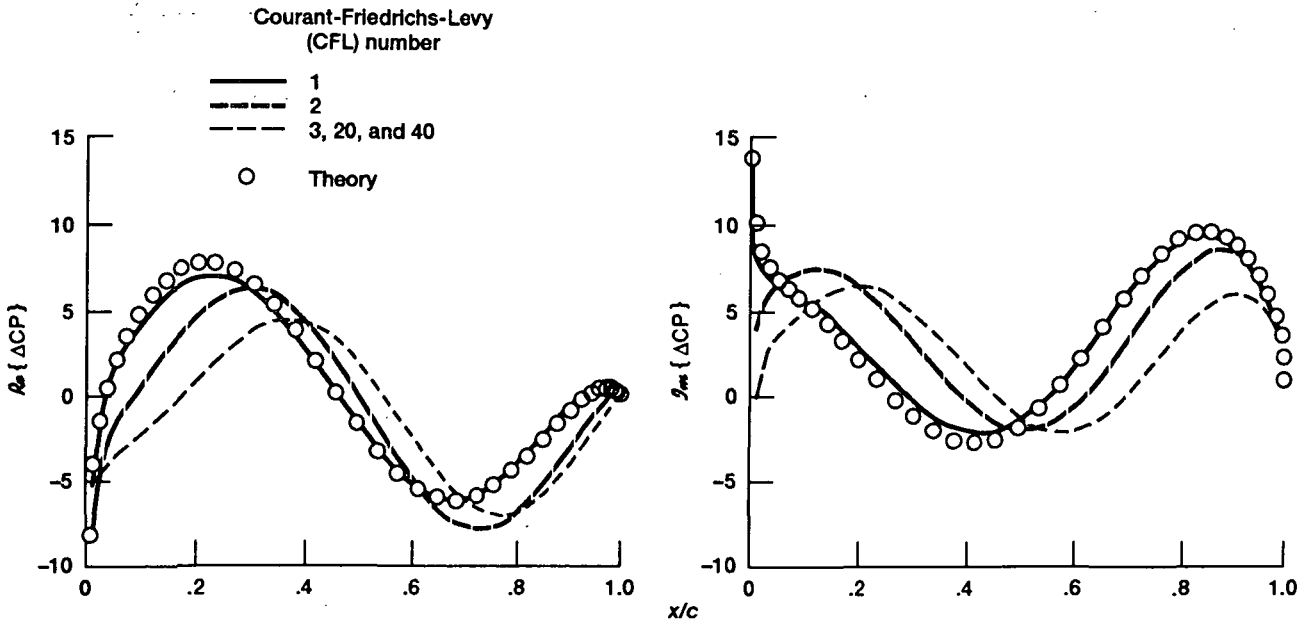
Figure 7.—Effects of time step on unsteady pressure distributions when a clustered grid is used.
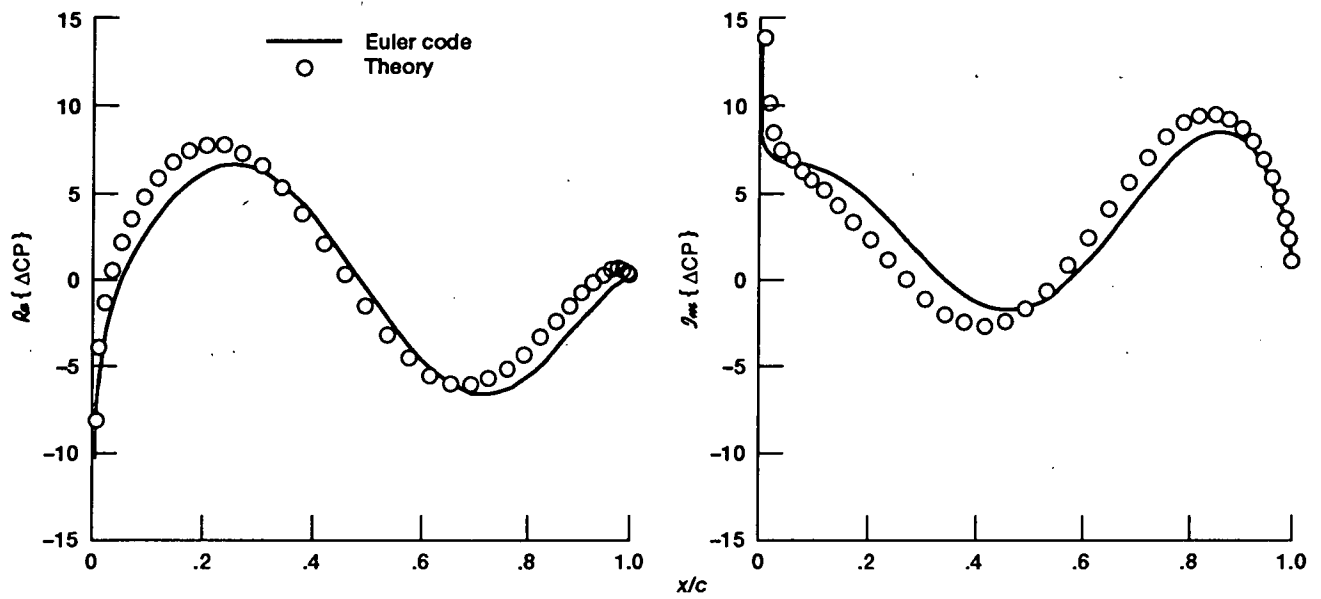
Figure 8.—Comparison of unsteady pressure distributions with linear theory for an optimal Euler solution.

REPORT DOCUMENTATION PAGE

1. AGENCY USE ONLY *(Leave blank)*	2. REPORT DATE 1991	3. REPORT TYPE AND DATES COVERED Technical Memorandum

4. TITLE AND SUBTITLE

Unsteady-Flow-Field Predictions for Oscillating Cascades

5. FUNDING NUMBERS

WU-535-03-10

6. AUTHOR(S)

Dennis L. Huff

7. PERFORMING ORGANIZATION NAME(S) AND ADDRESS(ES)

National Aeronautics and Space Administration
Lewis Research Center
Cleveland, Ohio 44135-3191

8. PERFORMING ORGANIZATION REPORT NUMBER

E-6613

9. SPONSORING/MONITORING AGENCY NAMES(S) AND ADDRESS(ES)

National Aeronautics and Space Administration
Washington, D.C. 20546-0001

10. SPONSORING/MONITORING AGENCY REPORT NUMBER

NASA TM-105283

11. SUPPLEMENTARY NOTES

12a. DISTRIBUTION/AVAILABILITY STATEMENT

Unclassified - Unlimited
Subject Category 02

12b. DISTRIBUTION CODE

13. ABSTRACT *(Maximum 200 words)*

The unsteady flow field around an oscillating cascade of flat plates with zero stagger was investigated by using a time-marching Euler code. This case had an exact solution based on linear theory and served as a model problem for studying pressure wave propagation in the numerical solution. The importance of using proper unsteady boundary conditions, grid resolution, and time step size was demonstrated for a moderate reduced frequency. Results show that an approximate nonreflecting boundary condition based on linear theory does a good job of minimizing reflections from the inflow and outflow boundaries and allows the placement of the boundaries to be closer to the airfoils than when reflective boundary conditions are used. Stretching the boundary to dampen the unsteady waves is another way to minimize reflections. Grid clustering near the plates captures the unsteady flow field better than when uniform grids are used as long as the Courant-Friedrichs-Levy (CFL) number is less than 1 for a sufficient portion of the grid. Finally, a solution based on an optimization of grid, CFL number, and boundary conditions shows good agreement with linear theory.

14. SUBJECT TERMS

Unsteady aerodynamics; Aeroacoustics; Aeroelasticity; Cascades; Computational fluid dynamics

15. NUMBER OF PAGES
24

16. PRICE CODE
A03

17. SECURITY CLASSIFICATION OF REPORT Unclassified	18. SECURITY CLASSIFICATION OF THIS PAGE Unclassified	19. SECURITY CLASSIFICATION OF ABSTRACT Unclassified	20. LIMITATION OF ABSTRACT

National Aeronautics and
Space Administration

Lewis Research Center
Cleveland, Ohio 44135

Official Business
Penalty for Private Use $300

NASA